E3S Web of Conferences **729**, 01003 (2026) https://doi.org/10.1051/e3sconf/202672901003
SPETM 2026

Impact of climatic variations on seasonal changes of earthing resistance

Samuel Nnamdi Onyedikachi*, *Omowunmi Mary* Longe

Department of Electrical and Electronic Engineering Science, APK Campus, University of Johannesburg, South Africa

Abstract. Seasonal soil-moisture flux causes time-varying soil resistivity and earthing resistance, which can compromise the safety of power-system earthing installations. Using representative sites in South Africa and Nigeria under comparable climates, this paper quantifies how temperature and relative humidity drive changes in topsoil suction and influence variation in subsoil resistivity and earthing resistance. The sites span four Köppen–Geiger climate classes: Aw (tropical savanna), BSh (hot semi-arid steppe), BWh (hot desert), and Cwb (subtropical highland). To study climate effects, a two-layer subsoil (silty top layer over sandy clay) with two earthing configurations: bare vertical rod and earthing enhancement material (EEM) embedded rod is modelled in COMSOL Multiphysics and simulated under the monthly suction values computed from the monthly average temperature and humidity data (1991-2021) of the sites. From post-processing, the resistance of bare and EEM-embedded rods was computed and compared with analytical equivalents. Results show consistent resistance reduction with EEM across months and climates. Earthing sites in BWh and BSh exhibit wider suction ranges and larger resistance variations than those in Aw and Cwb. Similar climate classes show comparable seasonal patterns, but their rainfall days and sunshine hours provide plausible contextual differences in resistance magnitude and variation.

1 Introduction

Earthing of electric power transmission components and systems is required to maintain a low-resistance path so that fault and lightning currents are dissipated safely into the ground [1]. The earthing resistance is governed by the (i) resistance of the electrode buried in the subsoil, (ii) the subsoil resistivity, and (iii) contact resistance between the electrode and the subsoil. In practice, soil resistivity and contact resistance dominate the total resistance because they vary with the hydraulic state of the soil, especially its water content and pore-water continuity [2].

Seasonal wetting and drying cycles modify soil suction, water content (effective saturation), and hence electrical conductivity. When suction increases (drier conditions), effective saturation reduces, and resistivity typically increases; the reverse occurs during wetter conditions. Therefore, earthing resistance is expected to vary seasonally, and in severe dry periods, it may exceed prescribed limits, leading to unsafe touch and step potentials during fault and lightning events [1].

A common mitigation is the use of earthing enhancement materials (EEMs), such as bentonite-based compounds, used to retain moisture around the electrode, reduce contact resistance, and improve earthing in high-resistivity sites [3]. However, EEM performance is also climate dependent. Environmental drying can reduce the water content of the EEM, increase its resistivity, and reduce the resistance-reduction benefit during the dry seasons or over time [4]. This makes it necessary to assess the performance of earthing systems under climate-driven seasonal variability rather than under a single assumed soil condition.

In earthing design and implementation, a common practice is to assume constant soil resistivity or apply correction factors for possible seasonal deviations. These approaches are often approximations that do not explicitly account for the physical soil state (suction, saturation, and conductivity pathways) that governs resistivity change [2]. A richer climate–subsoil assessment is therefore needed to quantify how climatic forcing drives seasonal resistivity and earthing resistance, and to understand how an EEM performs under those conditions.

Recent studies indicate a trend of using climate parameters especially atmospheric temperature to determine the microstructural, hydraulic, and mechanical behaviour of subsoil layers and as surrogate inputs to map underlying subsoil suction patterns [5-6].

Adopting similar approach this paper proposes a climate–suction–resistivity–earthing workflow to estimate and compare seasonal earthing behaviour at eight locations under representative climates in South Africa and Nigeria, using identical subsoil and earthing configurations to isolate climatic effects. The workflow while neglecting the influence of precipitation, assumes that subsoil resistivity variation is driven by atmospheric temperature and relative humidity. The study uses (i) a temperature-humidity based method in deriving monthly suction/pressure head from long-term monthly

* Corresponding author: 225213002@student.uj.ac.za

climate averages, (ii) a hydro–geoelectric coupling model to estimate subsoil resistivity and (iii) an analytical predictor for estimating earthing resistance from resistivity.

The aim of the study is to demonstrate how climatic variations drive seasonal changes in earthing resistance and to quantify the effectiveness of a clay-based EEM across different seasons, climates and locations in South Africa and Nigeria while ignoring its shrinkage effect. The study is undertaken with these objectives:

i. Compute monthly suction from monthly temperature and relative humidity (1991–2021) for eight sites across arid, semi-arid, tropical and subtropical climates.
ii. Model effective saturation as function of suction to estimate the resistivity of two-layer subsoil embedding a driven earth rod, with and without EEM in COMSOL Multiphysics.
iii. Compute and compare seasonal resistance patterns across matching Köppen–Geiger climates in South Africa and Nigeria and interpret differences using rainfall days and sunshine hours as contextual indicators of wetting frequency and drying potential.

2 Materials and methods

This section describes the study sites, climate classification, data sources, and the modelling workflow used to quantify seasonal changes in earthing resistance and performance. Monthly average temperature and relative humidity (1991–2021) were collected for representative locations in South Africa and Nigeria for four Köppen–Geiger climate classes: Aw (tropical savanna), BSh (hot semi-arid steppe), BWh (hot desert), and Cwb (subtropical highland). These climate variables were converted into monthly suction (pressure head) and applied as boundary conditions in a coupled hydro–geoelectric model of a two-layer subsoil with a vertical earth rod. Numerical simulations were performed in COMSOL Multiphysics for two earthing configurations: a bare rod and a rod embedded in a bentonite-based earthing enhancement material (EEM). Post-processed outputs were used to compute month-specific apparent/effective resistivity and earthing resistance, and analytical resistance expressions were used as verification checks against the simulation results.

2.1 Representative sites and climate classes

To evaluate the impact of suction on subsoil water content, monthly water potentials were computed from monthly averages of temperature and humidity data collected between 1991 and 2021 [7]. A supplementary data of rain days and sun hours for the period of 1999-2019 were collected to explain possible correlations between the wetting and drying cycles that affect soil water potential.

Table 1 summarises the climate data – monthly minimum-, maximum- and mean- temperatures (T_{min}, T_{max}, and $\overline{T}$) and relative humidity (R_{Hmin}, R_{Hmax}, and $\overline{R}_{H}$) and the means of rain days per month (RD/m), rain days per year (RD/y) and sunshine hours per day of the four selected locations in Nigeria and South Africa.

Table 1. Pseudo descriptive statistics of 1991 - 2021 climate data (temperature, relative humidity, rainfall days and sunshine hours) [7].

Site Code	South Africa				Nigeria			
	RB	BW	UP	JHB	ABJ	MD	ZI	GI
K-G CC	Aw	Bsh	Bwh	Cwb	Aw	Bsh	Bwh	Cwb
T_{min}	18.5	10.7	13.1	9.5	22.9	23.1	21.9	17.2
T_{max}	25.0	25.5	28.6	19.7	29.6	32.8	33.4	21.0
$\overline{T}$	21.9	19.1	21.5	15.9	26.0	28.0	28.4	18.9
RH_{mn}	0.68	0.28	0.21	0.35	0.26	0.12	0.09	0.32
RH_{mx}	0.76	0.51	0.44	0.68	0.87	0.79	0.73	0.90
$\overline{RH}$	0.72	0.40	0.31	0.54	0.60	0.39	0.31	0.67
RD/m	8.00	4.17	2.42	6.75	10.2	4.33	2.58	13.4
RD/yr	96.0	50.0	29.0	81.0	122	52.0	31.0	161
S-hr/d	7.72	10.5	10.6	9.13	7.39	10.4	10.6	8.42

K-GCC: Köppen–Geiger climate class, T_{min}, T_{max} and $\overline{T}$: are the minimum, maximum and mean temperatures (°C), RH_{min}, RH_{max} and $\overline{RH}$: are the minimum, maximum and mean relative humidity, RD/M: Rain days/month (mean), RD/Y: Rain days/year, SH/D: Sunshine (h/day mean), RB: Richard Bay, BW: Barkly West, UP: Upington, JHB: Johannesburg, ABJ: Abuja, MD: Maiduguri, ZI: Zari (in Borno State), GI: Guroji.

In all, eight sites were selected: four in South Africa and four in Nigeria. Each of these locations was chosen as a representative sample location of four climatic zones common in both countries. Based on Köppen–Geiger climate zone classifications, the zones are tropical savanna (Aw), hot semi-arid (BSh), hot desert (BWh), and subtropical highland (Cwb).

Aw climates are warm throughout the year and are defined mainly by a strong wet–dry season contrast: a pronounced summer rainy season and a drier winter season. Relative humidity and soil moisture typically rise sharply during the wet months and drop during the dry months.

BSh climates are hot with low to moderate rainfall, usually concentrated in a short-wet season, and a prolong period of high evaporation. Soil moisture is often intermittent and shallow, so the near-surface layer dries up quickly after rainfall.

BWh climates are very dry with rare, irregular rainfall, high temperatures, and strong solar radiation, leading to persistent drying.

Cwb climates occur at higher elevations and are generally milder than lowland tropics, with warm summers and cooler, drier winters. Rainfall is often summer-dominant, but the lower temperatures reduce evaporative demand compared with BSh/BWh.

2.2 Climate-suction formulations

The energy potential of subsoil water can be described by soil suction. Soil suction refers to the soil's affinity for water retention and represents the attractive strength of soil particle to water molecules. Monthly suction was derived from temperature and relative humidity using a humidity-based water potential equation expressed in Eq. 1 [8].

$$\psi_s = \psi_0 - \left(\frac{RT}{M}\right) \ln R_H \quad (1)$$

where ψ_s is water potential (MPa), ψ_0 is the reference potential (0 MPa for free water), R is the universal gas constant (8.314 J·K^{-1}·mol^{-1}), T is absolute temperature (K), M is the molar mass of water (0.01802 kg/mol), and R_H is relative humidity.

Under unsaturation condition, the approximate relationship between soil suction and hydraulic head (pressure head) is given by the standard head–potential relationship [9] expressed by Eq. 2.

$$h_p = -\left(\frac{\psi_s}{\rho_w g}\right) \quad (2)$$

where h_p is pressure head (m), ρ_w is water density (kg/m^3), and g is gravitational acceleration (m/s^2).

Table 2 shows some statistical descriptions of the suction (Mpa). To compute corresponding pressure head (m), ψ_s in Eq. (2) is in (Pa), implying that ψ_s from Eq. (1) is converted from MPa to Pa before applying Eq. (2). A more negative head indicates a drier condition.

Table 2. Suction statistics for eight sites under four climates computed from 1991–2021 monthly average temperature and relative humidity.

Site class	Köppen–Geiger climate code	Suction (MPa)		
		Min	Max	Mean
RB	Aw	37.69	52.07	44.00
BW	BSh	88.21	174.29	127.72
UP	BWh	108.46	215.11	162.49
JB	Cwb	52.11	140.30	85.50
AB	Aw	19.02	186.55	83.46
MD	BSh	32.56	296.65	157.24
ZI	BWh	43.65	335.90	190.69
GI	Cwb	14.11	154.53	63.19

K-GCC: Köppen–Geiger climate class, RB: Richard Bay, BW: Barkly West, UP: Upington, JHB: Johannesburg, ABJ: Abuja, MD: Maiduguri, ZI: Zari, GI: Guroji.

Tables 1 and 2 show that the driest climates (BWh and BSh) have the largest pressure-head ranges. For example, BWh (Zari, in Borno state, Nigeria) reaches a suction maximum of 335.90 MPa (−34.25 m pressure head), while Richard Bay (Aw, RSA) has a relatively narrow suction range 37.69–52.07 MPa (−5.31 to −3.84 m pressure head). This aligns with the observation that arid climates impose stronger and more persistent drying conditions on the near-surface layer, which increases resistivity and earthing resistance.

The rainfall-days and sunshine-hour indicators (Table 1) provide useful context: arid sites have few rainfall days per year and high sunshine hours, which implies fewer natural wetting opportunities and higher drying potential. Conversely, humid or temperate sites show more rainfall days, implying more frequent wetting cycles. These indicators help interpret persistence of dry-season peaks, although the suction in this workflow is directly computed from temperature and humidity (Eq. 1), not from rainfall infiltration.

2.3 Two-layer subsoil model and earthing configuration

Fig. 1 shows a vertical rod in a multi-layered soil. Each layer at its depth has its own composition, texture, water content and resistivity. Their influence on the earth rod depends on their contact or proximity to the buried earthing system. To reduce the complexity of multilayer resistivity, their influences are sometimes aggregated as a single homogeneous layer with a representative resistivity. However, the two-layer subsoil model offers better approximation to the actual profile of the soil and gives better results than the oversimplified homogeneous subsoil model. For this study, a two-layer subsoil model was used to model the eight earthing sites: a silty top layer of thickness 0.8 m over a sandy-clay bottom layer and a rod of radius r_e = 0.009525 m driven L_e = 3 m depth into the ground. For earthing composition with EEM, the driven rod is bounded by a cylindrical volume of radius r_m = 0.1152 m and length L_m = 3 m. The EEM was modelled with the hydraulic-electrical characteristics of a clay-based (bentonite) compound in line with EEM practice for grounding applications [3]. The geometric modelling and numerical simulations were performed using COMSOL Multiphysics and solved with finite element method (FEM) [10].

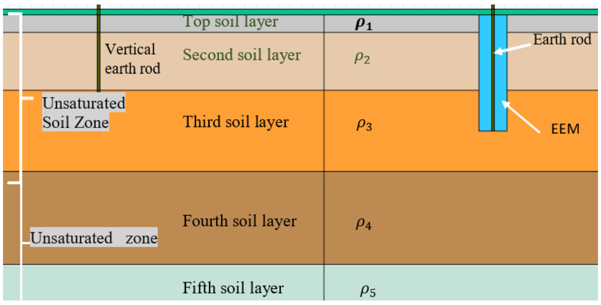

Fig. 1. Sectional view of multilayered subsoil with vertical bare rod (left) and rod embedded in earthing enhancement material (right).

2.4 Hydro–geoelectric coupling and resistivity evaluation

For the hydro-geoelectric model, the pressure head value is applied as a topsoil surface boundary condition to determine the water content of the subsoil and effective saturation. Details of the governing and coupling equations for the electric current distribution and fluid flow physics of unsaturated porous medium, as well as the modelling steps, boundary and initial conditions applicable in COMSOL Multiphysics modelling of the hydro-geoelectrical model with the vertical rod is extensively described in [10]. A more rigorous modelling approach would account for additional complexities of suction profile besides approximating subsoil water fluxes solely on suction.

However, to simplify the modelling process, a uniform suction profile was assumed within the unsaturated region of the subsoil. It is justified by the continuous profile of suction across subsoil layers that exist without discontinuity at the sublayer interfaces, and its relatively constant value at the depth of equilibrium suction [11].

For each subsoil layer, an effective saturation S_e is defined in terms of suction. S_e relates to the water content and textural characteristics of the porous medium as expressed in Eq. 3.

$$S_e(h_p) = \frac{\theta(h_P)-\theta_r}{\theta_s-\theta_r} \quad ()$$

where h_p (m) is the pressure head, θ_r and θ_s are the residual and saturated volumetric water contents, respectively. $\theta(h_p)$ is volumetric water content expressed as Eq. 4,

$$\theta(h_P) = \theta_r + \frac{\theta_s-\theta_r}{[1+(\alpha_h|h_p|)^{n_{vg}}]^{m_{vg}}} \quad (4)$$

where α_h (1/m) is the inverse of the air entry point, n_{vg} is the pore size distribution parameter and m_{vg} is the shape parameter ($m_{vg} = 1 - 1/n_{vg}$).

Water content-dependent electrical behaviour was interpreted using saturation–conductivity/resistivity relationships. Eq. 5 is an Archie-type behaviour that couples resistivity $\rho = \sigma^{-1}$ to the degree of saturation, S_e of soil [12].

$$\sigma(h_p) = A[S_e(h_p)]^{\,b} \quad (5)$$

where $\rho(h_p) = 1/\sigma(h_p)$, A is related to pore-water electrical conductivity and b is the saturation exponent or Archie's saturation index. The values of the coefficients A and b for subsoil layers and EEM were chosen based on values described [10] and restated in Table 3.

Table 3. Hydraulic and electrical parameters of subsoil layers and material for earthing enhancement material (EEM) [13].

Parameter	Silt	Sandy clay	EEM
θ_r [m³/m³]	0.034	0.090	0.030
θ_s [m³/m³]	0.460	0.360	0.5252
A [S/m]	0.0648	0.007386	0.930226
b [-]	1.132	2.247	1.753
K_s [m/s]	0.674E-6	0.333E-6	3.9E-6
α_h [m^{-1}]	1.600	2.700	0.784E-3
n_{vg} [-]	1.370	1.230	1.3587

θ_s and θ_r are saturated and residual volumetric water contents, A coefficient related to pore-water conductivity, b is the saturation index, K_s hydraulic conductivity of porous material, α_h is inverse of air-entry pressure head, n_{vg} is a pore size distribution parameter.

The resistance of the driven electrode in the 2-layer subsoil without and with EEM is evaluated from post processing simulation results based on equations specified in [10]. An analytical equivalent of the earthing resistance can be computed using the modified form of the formula Dwight-Sunde suggested and expressed in Eq. 6.

$$R_{ea} = \frac{\rho(h_p)}{2\pi L_e}\left[\ln\left(\frac{4L_e}{r_e}\right) - 1\right] \quad (6)$$

where $\rho(h_p)$ (Ωm) is the pressure head dependent resistivity of the homogeneous soil.

For an earthing configuration involving EEM, its resistivity ρ_m and volume around the vertical rod influences earthing resistance. This resistance R_{em} is estimated using Fagan's equation [14] expressed in Eq. 7.

$$R_{em} = \frac{\rho_m(h_p)}{2\pi L_m}\left(ln\frac{4L_m}{r_e} - 1\right) + \frac{\rho(h_p)-\rho_m}{2\pi L_e}\left(ln\frac{4L_e}{r_m} - 1\right) \quad (7)$$

Eq. 6 and 7 were used as analytical checks against the simulation outputs.

If the subsoil model is multi-layered, then an apparent or effective resistivity ρ_e replaces ρ in Eq. (6). Several suggestions exist in the literature for estimating ρ_e, and all involve the resistivity of the constituting layers. In this work, a formula is proposed for model-based effective resistivity. It was derived as a depth-weighted resistivity formulated based on the fractional depth of the driven rod in the layers of the n-layered subsoil. The proposed formula is expressed in Eq. 8.

$$\rho_e = \left[\frac{1}{L_e}\sum_{i=1}^{n_L}\frac{L_i}{\rho_i(h_p)}\right]^{-1} \quad (8)$$

where L_e is the vertical rod length, L_i is the length of the rod in i^{th} subsoil layer where $L_e = \sum L_i$, $\rho_i(h_p)$ is the resistivity of i^{th} subsoil layer, n_L number of subsoil layers such that $i = 1, 2, \cdots, n_L$.

3 Results and discussion

This section presents the simulated seasonal response of the two-layer subsoil and earthing system under the influence of monthly suction (pressure head) derived from the long-term climate averages. Results are organised to show (i) how pressure head drives monthly changes in effective/apparent resistivity, (ii) the corresponding seasonal variation of earthing resistance for the bare rod and the EEM-embedded rod, and (iii) a comparison of matched Köppen–Geiger climates between South Africa and Nigeria to explain similarities and differences in resistance magnitude and variability.

3.1 Apparent resistivity

Fig. 2 and Fig. 3 show combined plot of the monthly variation of apparent resistivity due to the monthly change of pressure head for the representative earthing sites under the four climatic zones common to South Africa and Nigeria.

Variation of monthly pressure head is shown as vertical bars scaled on the left vertical axis, while the corresponding variation in apparent resistivity is shown as curves scaled on the right vertical axis. Fig. 2 shows seasonal increases during dry months and reductions during wetter months.

The monthly apparent resistivity trends (Fig. 2–3) follow the seasonal trend of the pressure-head. In general, a more negative pressure head (stronger suction) reduces effective saturation and increases resistivity, consistent with established resistivity–moisture relationships in soils [2]. The layered model amplifies this behaviour because the top layer is more exposed to atmospheric elements and their variations, while the lower layer acts as a deeper reference that changes more slowly.

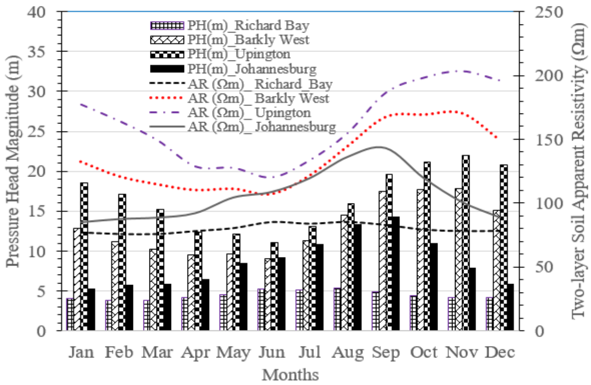

Fig. 2. Monthly variation of apparent resistivity of a two-layer subsoil model (silt over sandy clay) due to changes in pressure head of topsoil surface for four South African climates (1991 - 2021).

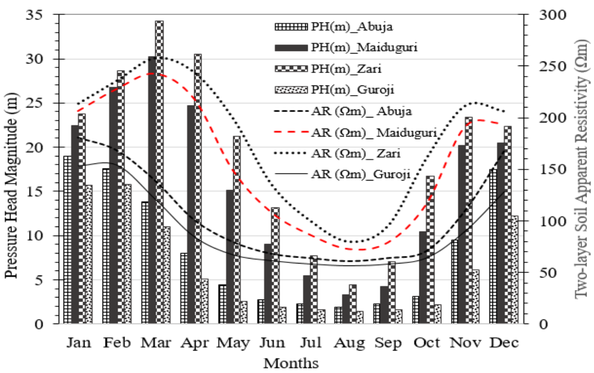

Fig. 3. Monthly variation of apparent resistivity of two-layer subsoil model (silt over sandy clay) due to changes in pressure head of topsoil surface for four Nigeria climates (1991 - 2021).

A key observation is that climates with a broader suction range (BWh, BSh) produce larger apparent resistivity fluctuations. This is consistent with the physical mechanism: wider suction swings imply larger changes in volumetric water content and pore connectivity, leading to larger changes in bulk conductivity and resistivity.

3.2 Earthing resistance without and with EEM

Earthing resistance results per site were summarised as monthly bar plots (Figures 4–5). Each plot shows bare-rod resistance (bars) and resistance with EEM (markers).

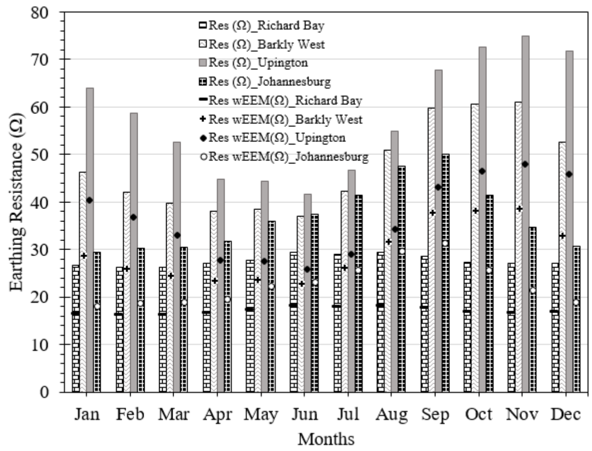

Fig. 4. Monthly earthing resistance (bars) and markers indicated resistance of the rod with earthing enhancement materials (EEM) for South African earthing sites and climate zones based on the Koppen-Geiger classification: Richard Bay (Aw), Barkly West (BSh), Upington (BWh), Johannesburg (Cwb).

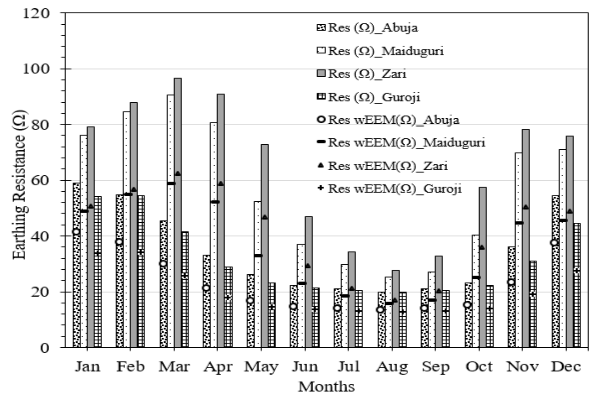

Fig. 5. Monthly earthing resistance (bars) and resistance (markers) with earthing enhancement materials (EEM) for Nigeria sites: Abuja (Aw), Maiduguri (BSh), Zari (BWh), Guroji (Cwb) under Koppen-Geiger classified climate zones indicated within the bracket.

To illustrate the climate-to-resistance workflow, a detailed description for Barkly Wesh (Bsh, RSA) is presented in Table 4. During months with more negative pressure head (stronger suction), both top- and bottom-layer resistivities increase, raising apparent resistivity and earthing resistance. The monthly resistance ranges from 37.01 Ω to 61.00 Ω. When EEM is added, resistance reduces to 22.83–38.50 Ω with a mean reduction of 37.76%. The key point is that EEM reduces the resistance, but it does not remove the seasonal shape; dry months still show higher resistance than wet months because the bulk soil resistivity increases under higher suction.

Table 5 summarises the resistance ranges and the mean values of resistance and percentage resistance reduction for the eight earthing sites based on the Multiphysics simulation output.

Table 4. Multiphysics simulation result showing the variation of subsoil resistivity and earthing resistance of the earthing site at Barkly West due to the influence of suction on the subsoil surface and computed from average monthly climate variation (1991 – 2021).

Month	h_p (m)	TLR	BLR	ER	Rsim	Rf	Rem
Jan	-12.9	54.3	278.5	132.6	46.2	43.2	28.7
Feb	-11.2	51.2	241.4	121.3	42.0	39.5	26.0
Mar	-10.2	49.3	223.6	115.0	39.7	37.5	24.5
Apr	-9.50	47.7	211.7	110.5	38.1	36.0	23.5
May	-9.70	48.1	214.3	111.5	38.5	36.3	23.7
Jun	-9.00	46.7	204.2	107.4	37.0	35.0	22.8
Jul	-11.3	51.3	243.0	121.8	42.2	39.7	26.1
Aug	-14.6	57.3	326.2	144.8	50.9	47.2	31.7
Sep	-17.4	61.8	443.2	167.5	59.9	54.6	37.7
Oct	-17.7	62.1	454.2	169.3	60.6	55.1	38.2
Nov	-17.8	62.3	460.7	170.3	61.0	55.5	38.5
Dec	-15.2	58.2	345.9	149.3	52.6	48.6	32.9

h_p (m): pressure head, TLR: top layer resistivity, BLR: bottom layer resistivity, ER: effective resistivity, Rsim; simulation-based Resistance, Rf: formula-based resistance, Rem: resistance of earthing enhancement material embedded rod, % RD: percentage resistance difference = (Rsim – Rf)/Rf, % RR: percentage resistance reduction.

Table 5. Multiphysics simulation result summary of the monthly resistance of bare driven earth rod and rod with earthing enhancement material (EEM) for eight sites under four climatic conditions.

Site Code	K-GCC	R (Ω) min–max	R (Ω) mean	R with EEM (Ω) min–max	Mean % resistance reduction EEM
RB	Aw	26.31–29.38	27.67	16.33–18.16	38.1
BW	Bsh	37.01–61.00	47.39	22.83–38.50	37.8
UP	Bwh	41.69–74.87	57.90	25.79–48.03	37.0
JB	Cwb	29.38–50.15	36.78	18.16–31.26	38.2
AB	Aw	21.55–65.46	37.50	13.59–41.55	37.4
MD	Bsh	25.14–90.55	57.05	15.65–58.56	36.9
ZI	Bwh	27.61–96.57	65.08	17.10–62.56	36.6
GI	Cwb	19.91–54.45	31.91	12.64–34.10	37.4

K-GCC: Köppen–Geiger climate class, R: resistance, RB: Richard Bay, BW: Barkly West, UP: Upington, JB: Johannesburg, ABJ: Abuja, MD: Maiduguri, ZI: Zari, GI: Guroji.

From Fig. 4 and 5, the earthing resistance result show that earthing sites in dry climates like BWh and BSh experience larger resistance fluctuations than earthing sites in tropical climates (Aw). This is consistent with the larger suction/pressure-head ranges (Table 2), which drive larger resistivity increases during dry months.

Secondly, although EEM provides a consistent reduction, the absolute resistance of the earthing system is climate dependent. The mean resistance reduction due to EEM is similar ≈ 36.6–38.2%, however, the absolute resistance during dry months can still be high in arid climates due to increasing resistivity of the surrounding subsoil within the region of influence of the earth electrode. This aligns with the understanding that EEM improves the local electrode region but cannot fully remove the impact of high-resistivity soil beyond the treated zone [15]. It is constructive to use an adequate volume of a high water-retaining EEM to ensure optimal performance. The volume of EEM used in this modelling was the critical volume: the volume beyond which no additional reduction is achieved, described in [13, 15].

Finally, earthing sites under humid climates can still attain seasonal peaks if humidity varies strongly. Abuja (Aw, NG) shows a wide suction range (19.02–186.55 MPa) despite being Aw, reflecting the strong seasonal swing in relative humidity (0.26–0.87). This produces noticeable resistance variation, indicating that humidity-driven suction can be a strong driver even where rainfall days are high.

3.3 Comparing performance under identical climates

The four Köppen–Geiger climate classification common to both countries provide a good basis for comparing the resistance of driven earth rods in similar climates across countries.

i. Hot desert (Bwh) - Upington and Zari: Both show high sunshine hours and few rainfall days (Table 1), with wide suction ranges (Table 2). Both produce high maximum resistance and strong seasonal variations (Table 3). Zari reaches a higher maximum resistance (96.57 Ω) than Upington (74.87 Ω), consistent with its wider suction range and lower RH minimum (0.09).
ii. Hot semi-arid (BSh) - Barkly West and Maiduguri: Both have moderate rainfall days and high sunshine hours. Maiduguri shows higher maximum resistance (90.55 Ω) than Barkly West (61.00 Ω), aligning with the larger suction and pressure-head range in Maiduguri (Table 2).
iii. Tropical savanna (Aw) - Richard Bay and Abuja: Richard Bay is humid year-round with a narrow suction range, giving the smallest resistance fluctuation (26.31–29.38 Ω). Abuja shows a much wider suction range driven by the strong seasonal humidity swing, which is reflected in its broader resistance range (21.55–65.46 Ω). This indicates that humidity-driven suction can dominate seasonal earthing behaviour even when rainfall days are high, if the dry season is characterised by very low humidity.
iv. Subtropical highland (Cwb) - Johannesburg and Guroji: Both places have moderate-to-high rainfall days and lower sunshine hours than the arid sites. Guroji has a slightly lower mean resistance (31.91 Ω) than Johannesburg (36.78 Ω), with a similar mean EEM benefit (≈37–38%). Guroji's high maximum relative humidity (0.90) and high rainfall days/year (161) support more frequent wetting conditions, which likely shorten the persistence of high-resistance months.

3.4 Study limitations and recommendations

To isolate and study climate effects, the study assumed identical subsoil layer profile and electrode at all sites. In practice, sites have different subsoil profiles, structures, composition, compaction, salinity and heterogeneity, which affect resistivity–moisture behaviour. Future work should model different combination of sublayer textures with other configurations and composition of earthing systems, such as grids, horizontal electrode and multiple rods.

Monthly suction values were computed from temperature and relative humidity (Eq. 1) data, while rainfall days and sunshine hours, which account for precipitation-infiltration and evaporation fluxes, were not included in the modelling. The omitted data should be included in future models to account for surface flux dynamics.

Using monthly climate averages smoothen short-duration extremes (storms, heat waves) that can significantly influence short-term resistance and safety margins, hence daily or hourly averages may be more appropriate.

Results were obtained for the numerical FEM model formulated with hydraulic and electrical parameters in COMSOL multiphysics. However, validation with field measurement is necessary and should be implemented in future work.

4 Conclusion

This paper shows that climatic variability can be mapped to seasonal earthing resistance changes through a physically interpretable workflow: beginning from temperature and relative humidity to suction and pressure head, then formulating saturation and resistivity and estimating earthing resistance - under four climates common to South Africa and Nigeria. Arid and semi-arid climates exhibit larger suction ranges and higher dry-season resistance peaks than humid climates. For these climate zones, the clay-based EEM offered consistent resistance reduction, but the absolute resistance remains strongly climate-dependent during dry months because the surrounding soil resistivity increases with suction. Comparison of similar Köppen–Geiger climates across the two countries show comparable seasonal patterns, but their rainfall-day frequency and sunshine hours correlates and explains the noticeable difference in resistance value and variation.

References

1. IEEE Std. 1410-, IEEE Guide for improving the lightning performance of electric power overhead distribution lines, (2011). https://doi.org/10.1109/IEEESTD.2011.57064
2. L. Fang, S. Shulin, and Z. Deheng, Correlation between electrical resistivity and suction for unsaturated coastal saline soil, IOP Conf. Ser. Earth Environ. Sci., vol. **362**, no. 1, p. 012143 (2019). https://doi.org/10.1088/1755-1315/362/1/012143
3. IEC 62561-7, Lightning protection system components (LPSC) – Part 7: Requirements for earthing enhancing compounds, (2018).
4. L. Zhe Kang, S. Chun Lim, U. Muhammad, F. Aman, and N. M. Nor, 'Comparative field assessment of grounding enhancement material for electrical earthing system', Bulletin EEI, vol. **13**, no. 5, pp. 3013–3020, (2024), https://doi.org/10.11591/eei.v13i5.7303
5. T. Chen, W. Fei, and G. A. Narsilio, Effective thermal conductivity of granular soils: a review of influencing factors and prediction models towards an investigation framework through multiscale characters, Can. Geotech. J., vol. **62**, pp. 1–17, (2025). https://doi.org/10.1139/cgj-2023-0465
6. G. Zhang et al., Multifractal time series analysis of grounding resistance in transmission line towers under cold-climate conditions, MATH, vol. **10**, no. 11, pp. 27985–28003 (2025), https://doi.org/10.3934/math.20251229
7. Climate data for cities worldwide. Accessed: Feb. 22, 2026. [Online]. Available: https://en.climate-data.org/
8. Z. Ter-Martirosyan and V. Bakhmisov, 'Boundary conditions for the problem of moisture transport in concrete', E3S Web Conf., vol. **263**, 03014 (2021). https://doi.org/10.1051/e3sconf/202126303014
9. S. N. Onyedikachi, C. Gomes, and J. Van Coller, Equations for predicting the volumetric water content affecting the resistivity of soil in the vicinity of a driven earth electrode in variably saturated homogeneous soil, in 2022 36th International Conference on Lightning Protection (ICLP), Cape Town, South Africa: IEEE, Oct. (2022), pp. 1–6. https://doi.org/10.1109/ICLP56858.2022.9942536
10. O. S. Nnamdi and G. Chandima, New method for modelling seasonal variation in resistance and performance of earthing systems, Energies, vol. **16**, no. 19, p. 7002, Oct. (2023). https://doi.org/10.3390/en16197002
11. A. H. Javid and R. Bulut, 'Equilibrium suction prediction model for subgrade soils in Oklahoma', Int. J. Geomech., vol. **23**, no. 10, 04023165 (2023). https://doi.org/10.1061/IJGNAI.GMENG-7076
12. Y. Fu, R. Horton, T. Ren, and J. L. Heitman, A general form of Archie's model for estimating bulk soil electrical conductivity, Journal of Hydrology, vol. **597**, p. 126160 (2021). https://doi.org/10.1016/j.jhydrol.2021.126160
13. S. N. Onyedikachi, Estimating resistance and performance of earthing systems electrode in variably saturated soil conditions, Ph.D. Dissertation, University of Witwatersrand, Johannesburg, 2024. [Online]. Available: https://wiredspace.wits.ac.za/items/6f00424d-a84d-4310-89d6-7bcaf9030538

14. S. N. Onyedikachi and C. Gomes, Modeling performance variation of earthing enhancement materials in different soils and conditions, in 2024 32nd Southern African Universities Power Engineering Conference (SAUPEC), Stellenbosch, South Africa: IEEE, Jan. (2024), pp. 1–6. https://doi.org/10.1109/SAUPEC60914.2024.10445044
15. J. Trifunovic, A Mathematical method for determining optimal quantity of backfill materials used for grounding resistance reduction, Mathematical Problems in Engineering, pp. 1–9, (2018). https://doi.org/10.1155/2018/4863702